A Search for H_2O Maser Emission in Southern AGN and Star Forming Galaxies – Discovery of a Maser in the Edge-on Galaxy IRAS F01063-8034

L. J. Greenhill,[1] S. P. Ellingsen,[2] R. P. Norris,[3] P. J. McGregor,[4] R. G. Gough,[3] M. W. Sinclair,[3] D. P. Rayner,[2] C. J. Phillips,[2,5] J. R. Herrnstein,[1,6] and J. M. Moran,[1]

ABSTRACT

We report the cumulative results of five surveys for H_2O maser emission at 1.35 cm wavelength in 131 active galactic nuclei (AGNs) and star-forming galaxies, conducted at the Parkes Observatory between 1993 and 1998. We detected one new maser, in the edge-on galaxy IRAS F01063-8034, which exhibits a single, ~ 0.1 Jy spectral feature at 4282 ± 6 km s^{-1} (heliocentric) with an unusually large 54 ± 16 km s^{-1} half-power full width. The centroid velocity of the emission increased to 4319.6 ± 0.6 km s^{-1} (38 ± 2 km s^{-1} width) over the 13 days between discovery and confirmation of the detection. A similarly broad linewidth and large change in velocity has been noted for the maser in NGC 1052, wherein jet activity excites the emission. Neither optical spectroscopy, radio-infrared correlations, nor infrared colors provide compelling evidence of unusual activity in the nucleus of IRAS F01063-8034. Since the galaxy appears to be outwardly normal at optical and infrared wavelengths, detection of an H_2O maser therein is unique. The maser emission is evidence that the galaxy harbors an AGN that is probably obscured by the edge-on galactic disk. The detection highlights the possibility that undetected AGNs could be hidden in other relatively nearby

[1]Harvard-Smithsonian Center for Astrophysics, 60 Garden St, Cambridge, MA 02138 USA; greenhill@cfa.harvard.edu .

[2]School of Mathematics and Physics, University of Tasmania, GPO Box 252-21, Hobart, Tasmania 7001 Australia.

[3]Australia Telescope National Facility, CSIRO, Epping Epping, NSW 2121 Australia.

[4]Research School of Astronomy and Astrophysics, Institute of Advanced Studies, Australia National University, Cotter Road, Weston Creek, ACT 2611, Australia.

[5]Current address: JIVE, Postbus 2, Dwingeloo 7990 AA The Netherlands.

[6]Current address: Renaissance Technologies, 25 E. Loop Dr., Stony Brook, NY 11790.

galaxies. No other maser emission features have been identified at velocities between 3084 km s^{-1} and 6181 km s^{-1}.

Subject headings: galaxies: active — galaxies: individual (IRAS F01063-8034) — galaxies: Seyfert — ISM: molecules — masers

1. Introduction

In active galactic nuclei (AGNs), H_2O maser emission can occur in the accretion disks of supermassive black holes and in shocks driven by jets and winds. The value of H_2O masers as astrophysical tracers is illustrated by interferometric maps that outline the structure of accretion disks with velocity resolutions < 1 km s^{-1} and angular resolutions < 1 milliarcsecond (mas). The best example is NGC 4258 (Miyoshi et al. 1995), followed by NGC 1068 (Greenhill & Gwinn 1997), and the Circinus galaxy (Greenhill et al. 2001a). Measurements of maser proper motions and line-of-sight accelerations also make possible estimates of geometric distance. For NGC 4258 the total fractional uncertainty in distance is $< 7\%$ (Herrnstein et al. 1999), which may contribute to the evaluation of systematic uncertainties in nongeometric measurement techniques, such as the Cepheid period-luminosity relation (Maoz et al. 1999; Mould et al. 2000).

In contrast, for the Circinus galaxy and NGC 1068 (Gallimore et al. 1996), interferometric observations show that *some* of the maser lines are associated with a wind or jet, while in the galaxies NGC 1052 (Claussen et al. 1998) and Mrk 348 (Peck et al. 2001) *all* the detected emission is displaced from the central engines entirely and apparently excited by prominent jets. These cases establish a second class of H_2O maser emission in AGNs. Most notable, the spectrum of the NGC 1052 maser exhibits a distinctive single broad emission feature (50-100 km s^{-1}), which is unlike the complexes of narrow maser lines seen toward accretion disks.

Twenty-two AGNs have been confirmed to exhibit H_2O maser emission: NGC 4945 (Dos Santos & Lepine 1979), Circinus galaxy (Gardner & Whiteoak 1982), NGC 1068, NGC 4258 (Claussen et al. 1984), NGC 3079 (Henkel et al. 1984; Haschick & Baan 1985), NGC 6240 (Henkel et al. 1984; Hagiwara, Diamond, & Miyoshi 2001), Mrk 1, Mrk 1210, NGC 1052, NGC 1386, NGC 2639, NGC 5506, NGC 5347, NGC 5793, ESO 103- G 34, IC 1481, IC 2560 (Braatz et al. 1996), IRAS F22265-1826 (Koekemoer et al. 1995), M 51 (Ho et al. 1987), NGC 3735 (Greenhill et al. 1997b), Mrk 348 (Falcke et al. 2000), and IRAS F01063-8034 (this work). However, detectable H_2O maser emission also arises in extragalactic star-forming regions, constituting a third class of extragalactic maser. Known sources lie in M 33

(Churchwell et al. 1977; Huchtmeier et al. 1978, 1988), IC 342 (Huchtmeier et al. 1978), M 82 (Claussen et al. 1984), IC10 (Henkel et al. 1986), NGC 253 (Ho et al. 1987), NGC 2146 (Tarchi 2001), and the Magellanic Clouds (Scalise & Braz 1981, 1982; Whiteoak et al. 1983; Whiteoak & Gardner 1986). Henkel et al. (1984); Claussen et al. (1984), and Huchtmeier et al. (1988) report several marginal detections in other galaxies. The apparent luminosities and spectral characteristics of these sources are comparable to masers in Galactic star-forming regions.

In past searches for extragalactic H_2O maser emission, more than 1000 galaxies have been observed. Two observations suggest masers are located preferentially in AGNs for which the geometry of the material in the central parsec is edge-on. First, *all* maser-host galaxies for which X-ray observations are available exhibit high X-ray obscuring columns $> 10^{23}$ cm^{-2} (e.g., Braatz et al. (1996)). Second, no masers are known in Seyfert 1 nuclei or other objects with relatively exposed broadline regions. Surveys of Seyfert 2 galaxies and low ionization nuclear emission regions (LINERs) achieve a 5-10% detection rate for nearby objects (e.g., Braatz et al. (1997)) that declines with distance, probably because of limited instrument sensitivity (IRAS F22265-1826 contains the most distant known maser, with $V_{helio} \sim 7570$ km s^{-1}, where we have assumed the optical definition of Doppler shift.)

Although high obscuring columns and edge-on geometries may describe many maser hosts, we note that the cases of NGC 1052 and Mrk 348 demonstrate that detectable maser emission can sometimes be associated with intense jet activity, and hence could in principle be observable in AGNs whose central parsecs are not viewed edge-on. In addition to gross geometric effects, the detection rates in past searches were probably also influenced by (1) the range of isotropic luminosity among masers, (2) chance alignments between (amplifying) maser regions and background nonthermal continuum sources along the line of sight, (3) warps in circumnuclear and accretion disks, (4) the survival of quiescent, warm, molecular gas in AGN environments, and (5) anisotropic beaming of maser radiation.

We present the results of five surveys conducted at the Parkes Observatory between 1993 and 1998. In Section 2 we discuss the observations and source samples. In Section 3, we discuss the discovery of H_2O maser emission in IRAS F01063-8034, new radio images, optical spectra, and the infrared colors of the galaxy. In Section 4, we conclude the discussion of whether IRAS F01063-8034 contains an AGN, and the implications thereof.

2. Parkes Survey

2.1. Observations

We observed the $6_{16} - 5_{23}$ transition of H_2O (λ1.3 cm) in position-switched total-power mode during five sessions between 1993 and 1998 (Table 1) with the Parkes 64-m radio telescope of the Australia Telescope National Facility. For most targets, to reduce the effects of atmospheric variability, we observed on and off-source scans (5 minutes each) through the same patches of sky. (We followed an off-source scan pointed 5^m west of the target, with two on-source scans, and a second off-source pointing 5^m east of the target to obtain a total on-source time of 10 minutes.) For galaxies in which we attempted to detect maser emission associated with star formation, and therefore observed multiple fields, we used pairs of fields as on-off pairs whenever practical.

To maximize the number of fields we could observe during the alotted telescope time, we collected enough data to permit a relatively coarse flux density calibration during each session, with the intention that we would refine that calibration following the detection of new H_2O masers. Hence, the calibration of noise levels in spectra obtained in 1993 - 1997 is only accurate to 30-50%, depending on the epoch. In general, we employed cross scans of calibrator sources to verify that pointing accuracy was generally better than $15''$, or about 20% of the primary beam. When feasible, we also estimated zenith opacities from system temperature data (typically $\lesssim 0.1$) and corrected for the elevation dependence of antenna sensitivity (Bourke 1994; Greenhill et al. 1997a).

In 1993, we used the dual channel prime focus maser receiver and 64 MHz (~ 850 km s^{-1}) digital autocorrelation spectrometer, which provided 1024 channels (~ 0.84 km s^{-1}) in each circular polarization. For each AGN, we centered the two observing bands approximately on the systemic velocity. For each star-forming region targeted, we centered the observing bands on the approximate line-of-sight velocity of the local interstellar medium, obtained from published H I or Hα spectroscopy. We grouped the observations so as to minimize the time spent retuning the 100 MHz-wide receiver bandpass (which required the antenna to be stowed). We adopted a ~ 5.7 Jy K^{-1} peak telescope sensitivity, based on prior antenna calibrations, which corresponds to an aperture efficiency of ~ 32% over the illuminated inner 44m of the antenna. The calibration uncertainty was roughly 30%.

Beginning in 1995, we used a new dual channel cryogenic high mobility electron transistor (HEMT) receiver and a 500 MHz bandwidth. We continued to use the 1024 channel autocorrelator and observed four contiguous 32 MHz bandpasses arranged to cover a broader 92 MHz or ~ 1200 km s^{-1} bandwidth with a channel spacing of ~ 0.84 km s^{-1}. Operations and calibration were conducted as in 1993, with a roughly 30% uncertainty in flux density

calibration.

In 1996, we observed four 32 MHz bands, two in each polarization, covering a reduced 52 MHz bandwidth, corresponding to ~ 700 km s^{-1}, with ~ 0.84 km s^{-1} channel spacing. The narrower instantaneous bandwidth permitted dual polarization operation that partly offset the loss in antenna gain caused by structural deformations resulting from installation of a new prime focus cabin. These observations were notable because of increased calibration uncertainty (50%) due to poor calibration of system temperature and the unknown elevation dependence of antenna gain associated with the new focus cabin.

In 1997 we again achieved a calibration accuracy of roughly 30% and estimated the peak antenna sensitivity to be 8.4 Jy K^{-1}, based on cross scans of Virgo A (21 Jy). We adopted this sensitivity to calibrate the 1996 data. We observed four 64 MHz bands, two in each polarization, with ~ 1.7 km s^{-1} channels. However, we observed each source twice, once with the bands offset to include largely redshifted velocities and once to include largely blueshifted velocities. In this way we synthesized a broader effective bandwidth than in previous sessions. For sources that had not been studied previously, we observed a 199 MHz effective bandpass (~ 2700 km s^{-1}) centered on the systemic velocity. For sources that had been studied previously (with spectrometer bandwidths on the order of 50 MHz), we increased the blue-red offset to cover effectively 244 MHz (~ 3300 km s^{-1}) and did not reobserve a 45 MHz band centered on the systemic velocity.

The observations in 1998 benefitted from the use of the new Parkes multi-beam correlator and from higher antenna gain following adjustment of the antenna surface. We obtained four contiguous 64 MHz bandpasses (~ 0.84 km s^{-1} channels) that we spread out to provide an instantaneous bandwidth of 236 MHz (~ 3100 km s^{-1}). Using observations of Virgo A, for which we adopted a flux density of 21 Jy and a 10% correction due to partial resolution of the source (Kuiper et al. 1987), we measured a 6.3 Jy K^{-1} antenna sensitivity. We corrected for atmospheric opacity and achieved a 20-30% calibration uncertainty overall.

2.2. Source samples

We employed several different source samples in the five Parkes surveys, including star forming galaxies, optically identified AGNs, and obscured AGNs. In 1993, we selected southern galactic nuclei ($\delta < -20^\circ$) with 100μm IRAS flux densities > 20 Jy. We also observed extragalactic star forming regions in the Sculptor and Centaurus A groups, the NGC 2997 and NGC 6300 associations, the Local Group, and several field galaxies (de Vaucouleurs 1975; Huchra & Geller 1982; Kraan-Korteweg & Tammann 1979). The observations of

southern Local Group galaxies complemented an earlier study of northern Local Group members (Greenhill et al. 1990). When we formulated the survey, nine of the eleven known extragalactic H_2O masers were associated with the 83 known IRAS galaxies with 100μm flux density > 50 Jy. However, in retrospect, discovery of these nine masers may have depended more on proximity of the galaxies to the Sun than on a (hoped for) direct physical relationship between maser emission (which arises in parsec scale structures) and IRAS far-infrared emission (which also originates on scales that are orders of magnitude larger). Among the larger number of H_2O masers known today, there is no apparent correlation. Galaxies with similar IRAS 100μm flux densities can have peak maser flux densities that differ by over an order of magnitude, and visa versa.

In 1995, we selected objects from two samples of active galaxies: (1) southern "radio-excess" IRAS galaxies (Roy & Norris 1997) and (2) nearby galaxies ($z < 0.09$; $\delta < +20^\circ$) that harbor hard X-ray sources ($E > 2$ keV) toward which substantial X-ray absorbing columns had been observered, using data from the EXOSAT (Turner 1988), HEAO-1 (Weaver et al. 1995), GINGA (Awaki 1991), and ASCA satellites (R. Mushotzky 1995, private communication). With respect to the first sample, radio emission that surpasses the radio-far infrared relation for normal galaxies is an indicator of activity (e.g., Condon, Anderson, & Broderick 1995; see Section 4) and can substitute for conventional optical identification when internal reddening is substantial. Koekemoer et al. (1995) observed 25 galaxies from a similar sample of northern radio-excess galaxies and detected the maser in IRAS F22265-1826. The second sample contained AGNs for which the measured absorbing columns were suggestive of the approximately edge-on geometries that seem to be a prerequisite for visible maser emission from accretion disks (see Braatz et al. (1996)).

In 1996, we observed galaxies detected both by IRAS and HEAO-1 (0.25-25 keV) and identified optically as Seyfert 2 objects by Kirhakos & Steiner (1990). We also selected targets from a sample of early-type galaxies whose compact radio cores (1-10 pc diameter) suggested the presence of AGNs. At least one quarter of the galaxies in this sample had been shown to be Seyfert 2 galaxies or LINERs (Slee et al. 1994).

In 1997, we again concentrated on Seyfert 2 galaxies and LINERs (< 9500 km s^{-1}) drawn from the CfA redshift survey (J. P. Huchra 1997, private communication), but searched specifically for high-velocity maser emission that previous surveys of southern galaxies could not have detected. The emphasis on bandwidth was motivated by the observation that in all galaxies with recognizable high and low-velocity maser emission (except NGC 4258), the high-velocity emission is stronger than the low-velocity emission, which may place narrow-band surveys at a relative disadvantage.

In 1998, we extended the high-velocity survey to galaxies identified by a cross-referencing

of the Parkes-MIT-NRAO (PMN) catalog (Wright et al. 1994) with the IRAS Faint Source Catalog (Moshir et al. 1992). These galaxies had known redshifts ($z < 0.085$) but in many cases had at best ambiguous spectroscopic identifications, because of substantial internal obscuration by gas and dust. However, as in our previous sample, the radio excesses were suggestive of nuclear activity. (We also included radio-excess objects ($\delta < 20^\circ$) taken from the Condon et al. (1995) sample that had not been investigated previously as possible sources of maser emission.)

3. Detection of an H_2O Maser in IRAS F01063-8034

We observed 131 AGNs (Table 2) and detected one new H_2O maser, in the edge-on galaxy IRAS F01063-8034 (Figure 1). Braatz et al. (1997) first noted a weak preference for observable maser emission in highly-inclined galaxies. With the detection of a maser in IRAS F01063-8034, 19 masers are known to lie in spiral galaxies, of which 9 have galactic inclinations $\gtrsim 70^\circ$. We have followed-up the detection by obtaining a confirming maser spectrum, radio images, and optical spectra.

3.1. The H_2O Maser Spectrum

We detected the H_2O maser with the Parkes antenna on 1998 August 27 and confirmed the detection on 1998 September 8 with the 70-m antenna of the NASA Canberra Deep Space Communications Complex at Tidbinbilla, Australia, which is several times more sensitive than Parkes (Figure 2). At Tidbinbilla, we used a cooled, wide-band HEMT receiver and a single polarization, 20 MHz bandwidth (270 km s^{-1}), 16384 channel correlation spectrometer in position-switched total-power mode. We convolved the spectra with a 16 channel wide boxcar function to obtain a 0.26 km s^{-1} channel spacing. In order to search for emission more than ~ 10 MHz away from the line we observed first, we tuned the receiving system to several band-center velocities and covered the range 4100 to 4850 km s^{-1}, achieving an RMS noise level of ~ 30 mJy in each spectral channel. (The system temperature changed by 30-40% from day to day possibly because of weather conditions. We conservatively estimate that the calibration is uncertain by perhaps 50%.)

The line profile of the emission observed at Parkes is well fitted by a Gaussian model with a 0.09 ± 0.02 Jy peak, 4282 ± 6 km s^{-1} centroid, and 54 ± 16 km s^{-1} half-power full width (Figure 2). A model fitted to the emission observed at Tidbinbilla has a 0.113 ± 0.004 Jy peak, 4319.6 ± 0.6 centroid, and 38 ± 2 km s^{-1} half-power full width (where we quote

statistical errors). The velocity shift of 38 km s^{-1} over 13 days is almost unprecedented. The only other similar occurence has been in NGC 1052, where the single emission feature jumped by 45 km s^{-1} between two observations 5 months apart (Braatz et al. 1996).

We have confirmed the calibration of the velocity scales for our Parkes and Tidbinbilla spectra separately at the < 1 km s^{-1} level. For the Parkes data, we have compared the measured heliocentric velocities of two widely separated lines in a spectrum of the H_2O maser in the Circinus Galaxy, obtained during the 1998 August observations reported here, to an independent spectrum created from VLBI data recorded in 1998 June. For the Tidbinbilla data, we have compared the centroid velocity for a persistent, isolated spectral feature of the Mrk 1210 H_2O maser measured on 1997 November 15 with that measured with antennas at Effelsberg and GreenBank between 1993 and 1996 (Braatz 1996; Braatz et al. 1996). Ultimately, the velocity scale for both stations is derived directly from the observed band-center sky frequency determined by the tuning of receiver elements. At Tidbinbilla in particular, this is directly set by the observer, and hence, the spectrometer calibration is as robust as that of the more widely tested Parkes system.

The mechanism responsible for the distinctive broad, centrally-peaked H_2O maser lines associated with strong jet activity (i.e., NGC 1052 and Mrk 348) is not well understood. We speculate that the lines may be composites of narrower, spatially distinct features. Such composites are seen toward some AGN of late-type systems, for which spectral features narrower than a few km s^{-1} sometimes blend together to form broad but irregular complexes (e.g., NGC 1068). Where maser excitation is tied to jets, individual spectral components could correspond to individual shocks in entrained or ambient material. However, the largely smooth, centrally peaked maser line profiles of these systems contrast with the irregular appearance of maser line complexes (more commonly) associated with AGNs. We suggest that the contrast could reflect the difference between maser amplification in accretion disks, which have well ordered dynamics, and amplification in jet entrained material, which has relatively chaotic dynamics. Furthermore, we note that a third example of broad maser emission, IRAS F22265-1826, has been resolved into at least four clumps distributed over ~ 1 pc with individual line widths of tens of km s^{-1} (Greenhill et al. 2001b), although association of this maser with an underlying jet is less certain than it is for NGC 1052 and Mrk 348.

The 45 km s^{-1} shift in the maser line velocity of NGC 1052 (in < 5 months) is interesting. We argue that such variation could be typical in masers driven by jet-activity, for which intrinsically fast fluctuations in a (relativistic) jet, or in its interaction with the surrounding medium, may cause new centers of emission to rise, others to decline, and the composite line to shift in velocity. The maximum possible shift would at least depend on the velocity

dispersion of the entrained material or bulk flows in ambient material. Although the apparent persistence of a smooth, centrally peaked line profile in NGC 1052 should constrain this model, at present, there is insufficient data from spectroscopic monitoring to do so.

We suggest that IRAS F01063-8034 contains a previously undetected AGN because of the broad maser line profile and unusual variation in velocity, which are also observed in NGC 1052. Abrupt changes in velocity are difficult to understand in the context of two alternate models, maser emission from a thin accretion disk, as in NGC 4258, or from a starburst, as in NGC 253 and M 82. Accretion disks that support maser emission are slowly varying structures, and the apparent luminosities of known masers that are associated with star formation are relatively small. (The flux density of the M 82 maser, scaled to a nominal distance of 57 Mpc, assuming $cz \sim 4300$ km s^{-1} and $H_\circ = 75$ km s^{-1} Mpc^{-1}, is ~ 300 times weaker than IRAS F01063-8034.)

3.2. Optical Spectroscopy

We obtained optical spectra of IRAS F01063-8034 with the Double Beam Spectrograph (Rodgers, Conroy, & Bloxham 1988) on the Australia National University 2.3 m telescope at Siding Spring Observatory on 2000 October 1. The $4''$ slit was aligned with the minor axis of the galaxy. The B600 and R600 gratings (in the blue and red arms of the spectrograph, respectively) provided velocity resolutions of ~ 300 km s^{-1} from 3800–5350 Å and ~ 200 km s^{-1} from 5700–7500 Å. A Ne–Ar arc lamp spectrum obtained 12 hr prior to the astronomical observation provided calibration of the wavelength scale. Analysis of OH emission in the extracted sky spectrum permitted some refinement of the velocity calibration for the red spectrum (Osterbrock et al. 1996); after calibration with 22 sky emission lines, uncertainty in the wavelength calibration was 0.37 Å or ~ 17 km s^{-1} (1σ). The galaxy spectra were flux calibrated using a spectrum of EG 131 obtained on the same night and the absolute flux calibration of Bessel (1999). Figure 3 shows the blue and red spectra for the central $14\farcs4$ (16 pixels) along the slit.

The continuum light of late-type stars dominates the minor axis optical spectrum of IRAS F01063-8034 (Figure 3). The prominent central dust lane (Figure 1) almost completely obscures the disk plane so most of these stars must belong to the central bulge population. Weak emission is seen near Hα/[N II], but no other emission lines are apparent, which makes optical spectroscopic identification of nuclear activity difficult.

Based on a detailed analysis of the spectrum (Figure 4) we suggest that the observed emission line is [N II] λ6583, in which case the implied heliocentric systemic velocity is

4285 ± 35 km s^{-1}. The velocity inferred from Na I D and Mg I b λ5183 absorption lines are 4246 ± 50 km s^{-1} and ~ 4140 km s^{-1}, respectively, though we emphasize that the zero point of the blue spectrum is uncertain, because there were not enough sky emission lines to refine the wavelength calibration. The three line velocities agree reasonably well with each other, which precludes identification of the emission line as Hα, for which the implied redshift would be ~ 1050 km s^{-1}. Prior estimates of the systemic velocity are 4249 ± 27 km s^{-1} (Dacosta et al. 1991) and 5047 ± 21 km s^{-1} (Sadler 1984), both of which rely on cross correlation of stellar absorption features. (Dacosta et al. may have also modelled the lone emission line reported here but it would contribute relatively little to their published weighted mean velocity. We note that Phillips et al. (1986) report an early failure to detect [N II] emission.)

The probable identification of [N II] emission provides some additional evidence for there being an AGN in IRAS F01063-8034, specifically a LINER. The [N II] line flux is $3.4 \pm 0.3 \times 10^{-15}$ erg s^{-1} cm^{-2} (comparable to the Phillips et al. (1986) upper limit), and the 3σ upper limit on Hα emission is $\sim 1.2 \times 10^{-15}$ erg s^{-1} cm^{-2}, from which we estimate that the familiar AGN emission line ratio diagnostic $\log([\mathrm{N\,II}]\lambda 6583/\mathrm{H}\alpha)$ is $\gtrsim 0.44$. This is characteristic of LINERs among early-type galaxies (Veilleux & Osterbrock 1987; Phillips et al. 1986). Although the Hα emission flux may be artificially low because of stellar Hα absorption, the effect is likely to be small because there is only marginal evidence for Hβ absorption (Figure 3) and no indication of higher Balmer lines in absorption.

3.3. Radio Images

We made radio snapshots of IRAS F01063-8034 with the Australia Telescope Compact Array (ATCA) at 3.5 cm and 6.3 cm wavelength in 1998 January and February with the 6C and 6B configurations, respectively (18 minutes on-source in each of two 12 hour tracks). We calibrated the phase data with respect to the calibrator 0252-712 and the amplitude data with respect to 1934-638, for which we adopted flux densities of 2.8 Jy at 3.5 cm and 5.8 Jy at 6.3 cm. The angular resolutions were $\sim 1''$ and $\sim 2''$ at the two wavelengths, respectively.

At each wavelength, emission is limited to a weak source associated with the galactic nucleus (Figure 1; Table 3). The observed flux density at 6.3 cm is significantly smaller than the 81 ± 7 mJy reported in the PMN catalog (Wright et al. 1994). However, this is at least in part the result of confusion in the Parkes $> 1'$ beam, because there is a second source at about $\alpha_{2000} = 01^h07^m04\overset{s}{.}7$, $\delta_{2000} = -80°17'04''$. Its flux density is ~ 13 mJy and ~ 27 mJy at 3.5 and 6.3 cm, respectively.

We included IRAS F01063-8034 in our survey because its 6.3 cm radio flux density in

the PMN catalog (Wright et al. 1994) exceeded that expected based on its IRAS 60 μm flux density, which suggested that the radio emission was powered by an AGN. However, the weaker observed radio flux density isolated to the nucleus begs the question of whether there is really any radio-excess (and whether the galaxy should have been included in our surveys - twice). It is clear from Figure 5 that IRAS F01063-8034 actually lies on the well known radio-FIR correlation for starburst galaxies and radio-quiet AGNs, which underscores that there is no radio-excess and no further evidence of activity.

3.4. Infrared Colors

AGNs have been identified with some success by analyses of infrared colors. Nuclear activity heats dust that creates excess 12 and 25 μm emission and warm IRAS 25–60 μm colors (Low et al. 1988; de Grijp, Miley, & Lub 1987; de Grijp et al. 1992). For IRAS F01063-8034, $\log(F_{60\mu m}/F_{25\mu m}) = 1.023$, which is much cooler than the 0.6 upper limit used by Low et al. (1988) to identify (warm) candidate AGNs. Rush, Malkan, & Spinoglio (1993) used the IRAS Faint Source Catalog (Moshir et al. 1992) to investigate the far-infrared colors of their Extended 12 Micron Galaxy Sample. On a two color diagram IRAS F01063-8034 lies at the extreme cool end of the locus of non-Seyfert galaxies (Figure 6), indicating that its IRAS flux densities are dominated by cool dust typical of normal galaxies; there is no indication of the warm far-infrared emission typical of many Seyfert galaxies. While some Seyfert galaxies do occupy this same region of the far-infrared two-color diagram, these are likely to be objects in which star formation in the host galaxy dominates the far-infrared emission from the Seyfert nucleus. The same may be true for IRAS F01063-8034 where we know from the optical spectrum that any nuclear activity could be weak or highly obscured at optical wavelengths, probably by the edge-on galactic dust disk.

4. Conclusion

No normal galactic nuclei have been known to host H_2O maser emission, yet IRAS F01063-8034 *appears* to be a normal galaxy. High excitation optical lines are absent and common measures that rely on estimates of nuclear far-infrared or radio continuum flux densities do not betray substantial activity. However, variable H_2O maser emission that we speculate is excited by jet activity (as in NGC 1052 and Mrk 348) and the putative [N II] emission, are suggestive of nuclear activity in IRAS F01063-8034. We propose that this galaxy contains a heavily obscured AGN, and that it may represent a larger class of AGNs undetectable in optical and infrared surveys, because of the inclinations of galactic disks or smaller scale

optically thick structures. X-ray spectroscopic observations may resolve the nature of the IRAS F01063-8034 nucleus, but at present, it is the only AGN identified first by detection of H_2O maser emission. Apparently normal galaxies that are highly inclined may be profitable targets for new surveys intended to detect extragalactic H_2O maser emission.

We thank Harry Fagg, Euan Troup, Warwick Wilson, and the Parkes engineering staff for their dedication and assistance during the 5 years of observation, in particular with the maser receiver system, correlator, and signal processing electronics. Paul Harbison and Edward King assisted with collection and reduction of Tidbinbilla data. We thank Michael Bessell for obtaining the optical spectrum and both Michael Dopita and Jim Braatz for informative discussions. We also acknowledge the public service of Jim Braatz who has maintained a cumulative catalog of galaxies that have been observed in searches for new H_2O maser sources (http://www.gb.nrao.edu/∼jbraatz/H2O-list.html). We are grateful to Lee Simons for substantial assistance in constructing Table 3 and cross-checking the contents with available databases. SPE acknowledges financial support from the Australian Research Council. This research has made use of the NASA/IPAC Extragalactic Database (NED) which is operated by the Jet Propulsion Laboratory, California Institute of Technology, under contract with the National Aeronautics and Space Administration.

REFERENCES

Awaki, H. 1991, Ph.D. thesis, Nagoya Univ.

Bessell, M. S. 1999, PASP, 111, 1426

Bourke, T. L. 1994, M.Sc. thesis, Univ. of New South Wales

Braatz, J. A. 1996, Ph.D. Dissertation, Univ. of Maryland

Braatz, J. A., Wilson, A. S., & Henkel, C. 1996, ApJS, 106, 51

Braatz, J. A., Wilson, A. S., & Henkel, C. 1997 ApJS, 110, 321

Churchwell, E., Witzel, A., Pauliny-Toth, I., Sieber, W., Huchtmeier, W., & Roland, J. 1997, A&A, 54, 969

Claussen, M. J., Heiligman, G. M., & Lo, K.-Y. 1984, Nature, 310, 298

Claussen, M. J., Diamond, P. J., Braatz, J. A., Wilson, A. S., Henkel, C. 1998, ApJ, 500, L129

Condon, J. J., Anderson, & Broderick, 1995, AJ, 109, 2318

Dacosta, L. N., Pellegrini, P. S., Davis, M., Meiksin, A., Sargent, W. L. W., Tonry, J. L. 1991, ApJS, 75, 935

de Grijp, M. H. K., Miley, G. K., & Lub, J. 1987, A&AS, 70, 95

de Grijp, M. H. K., Keel, W. C., Miley, G. K., Goudfrooij, P., & Lub, J. 1992, A&AS, 96, 389

de Vaucouleurs, G. 1975, in Stars and Stellar Systems, vol. 9: Galaxies and the Universe, A. Sandage, M. Sandage, & J. Kristian eds., (Chicago: University of Chicago), ch 14

de Vaucouleurs, G., de Vaucouleurs, A., & Corwin, H. G. Jr. 1976, Second Reference Catalogue of Bright Galaxies (Austin: University of Texas), p. 14

Dos Santos, P. M., & Lepine, J. R. D. 1979, Nature, 278, 34

Falcke, H., Henkel, C., Peck, A. B., Hagiwara, Y., Almudena, P. M., & Gallimore, J. F. 2000, A&A, 358, L17

Gallimore, J. F., Baum, S. A., O'Dea, C. P., Brinks, E., & Pedlar, A. 1996, ApJ, 462, 740

Gardner, F. F., Whiteoak, J. B 1982, MNRAS, 201, P13

Greenhill, L. J., Moran, J. M., Reid, M. J., Gwinn, C. R., Menten, K. M., Eckart, A., & Hirabayashi, H. 1990, ApJ 364, 513

Greenhill, L. J., Ellingsen, S. P., Norris, R. P., Gough, R. G., Sinclair, M. W., Moran, J. M., & Mushotzky, R. 1997a, ApJ, 474, L103

Greenhill, L. J., Gwinn, C. R. 1997, Ap&SS, 248, 261

Greenhill, L. J., Herrnstein, J. R., Moran, J. M., Menten, K. M., & Velusamy, T. 1997b, ApJ, 486, L15

Greenhill, L. J., et al. 2001a, in Proc IAU Symp. 205, Galaxies and Their Constituents at the Highest Angular Resolutions, eds. R. Schilizzi, S. Vogel, F. Paresce, & M. Elvis (ASP Conf. Ser.; San Francisco: ASP), 334-337

Greenhill, L. J., Moran, J. M., & Henkel, C. 2001b, in prep.

Hagiwara, Y., Diamond, P. J., & Miyoshi, M. 2001, A&A, submitted

Haschick, A. D. & Baan, W. A. 1985, Nature, 314, 144

Henkel, C., Güsten, R., Wilson, T. L., Biermann, P., Downes, D., & Thum, C. 1984, A&A, 141, L1

Henkel, C., Wouterloot, J. G. A., & Bally, J. 1986, A&A 155, 193

Herrnstein, J. R., et al. 1999, Nature, 400, 539

Ho, P. T. P., Martin, R. N., Henkel, C., & Turner, J. L. 1987, ApJ, 320, 663

Huchra, J. P. and Geller, M. J. 1982, ApJ, 257, 423

Huchtmeier, W. K., Witzel, A., Kuehr, H., Pauliny-Toth, I. I., & Roland, J. 1978, A&A, 64, L21

Huchtmeier, W. K., Eckart, A., & Zensus, A. J. 1988, A&A, 200, 26

Kirhakos, S. D. & Steiner, J. E. 1990, AJ, 99, 1722

Koekemoer, A. M., Henkel, C., Greenhill, L. J., Dey, A., van Breugel, W., Codella, C., & Antonucci, R. 1995, Nature, 378, 697

Kraan-Korteweg, R. C., & Tammann, G. A. 1979, Astron Nachr, 300, 181

Kuiper, T. B. H., Peters, W. L., III, Forster, J. R., Gardner, F. F., & Whiteoak, J. B. 1984, PASP, 99, 107

Low, F. J., Huchra, J. P., Kleinmann, S. G., & Cutri, R. M. 1988, ApJ, 327, L41

Maoz, E., et al. 1999, Nature, 401, 351

Miyoshi, M., Moran, J., Herrnstein, J., Greenhill, L., Nakai, N., Diamond, P., & Inoue, M. 1995 Nature, 373, 127

Moshir, M. et al. 1992, Explanatory Supplement to the IRAS Faint Source Survey, Version 2, JPL D-10015 8/92 (Pasadena:JPL)

Mould, J. R., et al. 2000, ApJ, 529, 786

Osterbrock, D. E., Fulbright, J. P., Martel, A., Keane, M. J., Trager, S. C., & Basri, G. 1996, PASP, 108, 277

Peck, A. P., Falcke, H., Henkel, C., Menten, K., Hagiwara, Y., Gallimore, J., & Ulvestad, J. 2001, in Proc IAU Symp. 206, Cosmic Masers: From Protostars to Black Holes eds. V. Migenes (ASP Conf. Ser.; San Francisco: ASP), in press

Phillips, M. M., Jenkins, C. R., Dopita, M. A., Sadler, E. M., & Binette, L. 1986, AJ, 91, 1062

Rodgers, A. W., Conroy, P., & Bloxham, G. 1988, PASP, 100, 626

Roy, A. L., & Norris, R. P. 1997, MNRAS, 289, 824

Rush, B., Malkan, M. A., & Spinoglio, L. 1993, ApJS, 89, 1

Sadler, E. M. 1984, AJ, 89, 23

Scalise, E., & Braz, M. A. 1981, Nature, 290, 36

Scalise, E., & Braz, M. A. 1982, AJ, 87, 528

Slee, O. B.,Sadler, E. M., Reynolds, J. E., & Ekers, R. D. 1994, MNRAS, 269, 923

Tarchi, A. 2001, Ph.D. thesis, Univ. of Bonn

Turner, T. J. 1988, Ph.D. thesis, Univ. of Leicester

van den Bergh, S. 1988, PASP, 100, 344

Veilleux, S., & Osterbrock, D. E. 1987, ApJS, 63, 295

Weaver, K. A., Arnaud, K. A., & Mushotzky, R. F. 1995, ApJ, 447, 121

Whiteoak, J. B., & Gardner, F. F. 1986, MNRAS, 222, 513

Whiteoak, J. B., Wellington, K. J., Jauncey, D. L., Forster, J. R., Caswell, J. L., & Batchelor, R. A. 1983, MNRAS, 205, 275

Wright, A. E., Griffith, M. R., Burke, B. F., & Ekers, R. D. 1994, ApJS, 91, 111

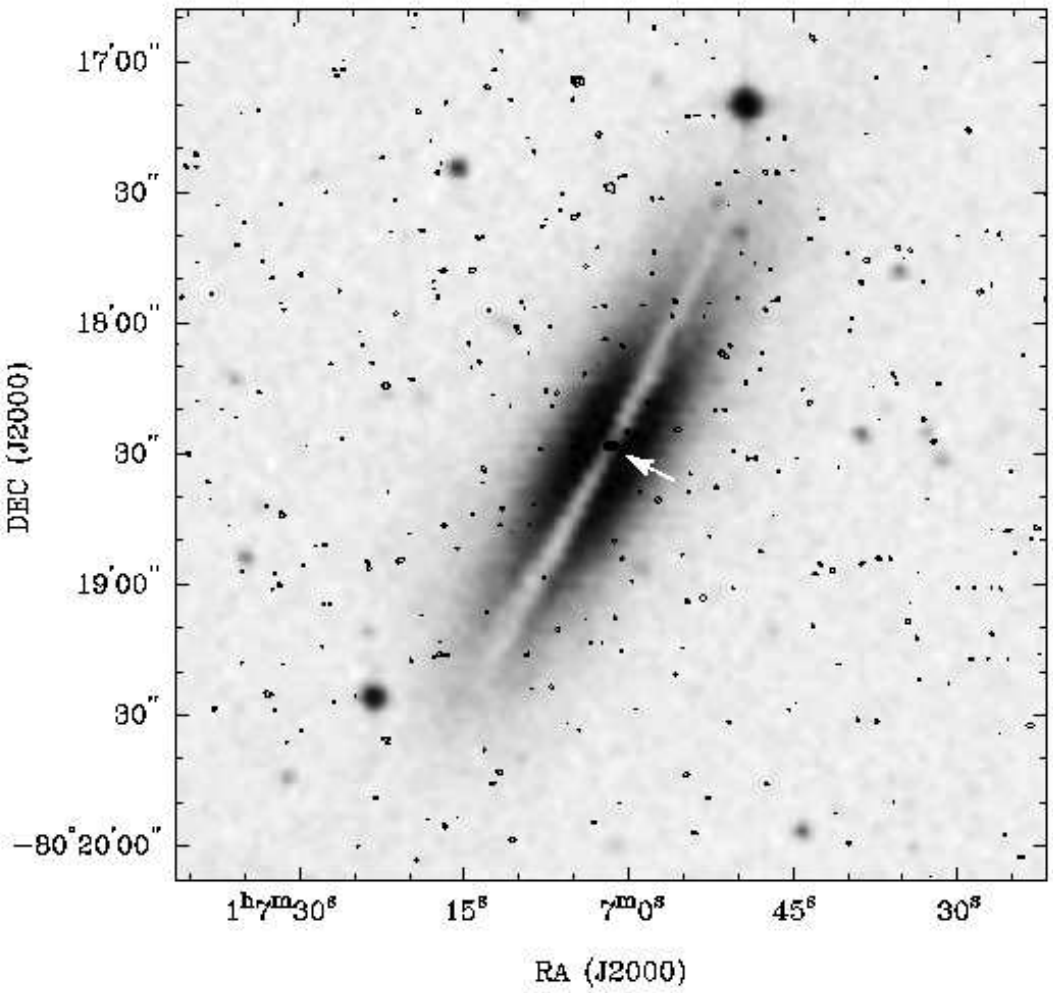

Fig. 1.— Digitized Sky Survey blue image of IRAS F01063-8034 (*gray scale*) with 1″ resolution and 4 cm wavelength continuum ATCA snapshot superposed (*contours*). The arrow indicates the contours that mark the nuclear radio source.

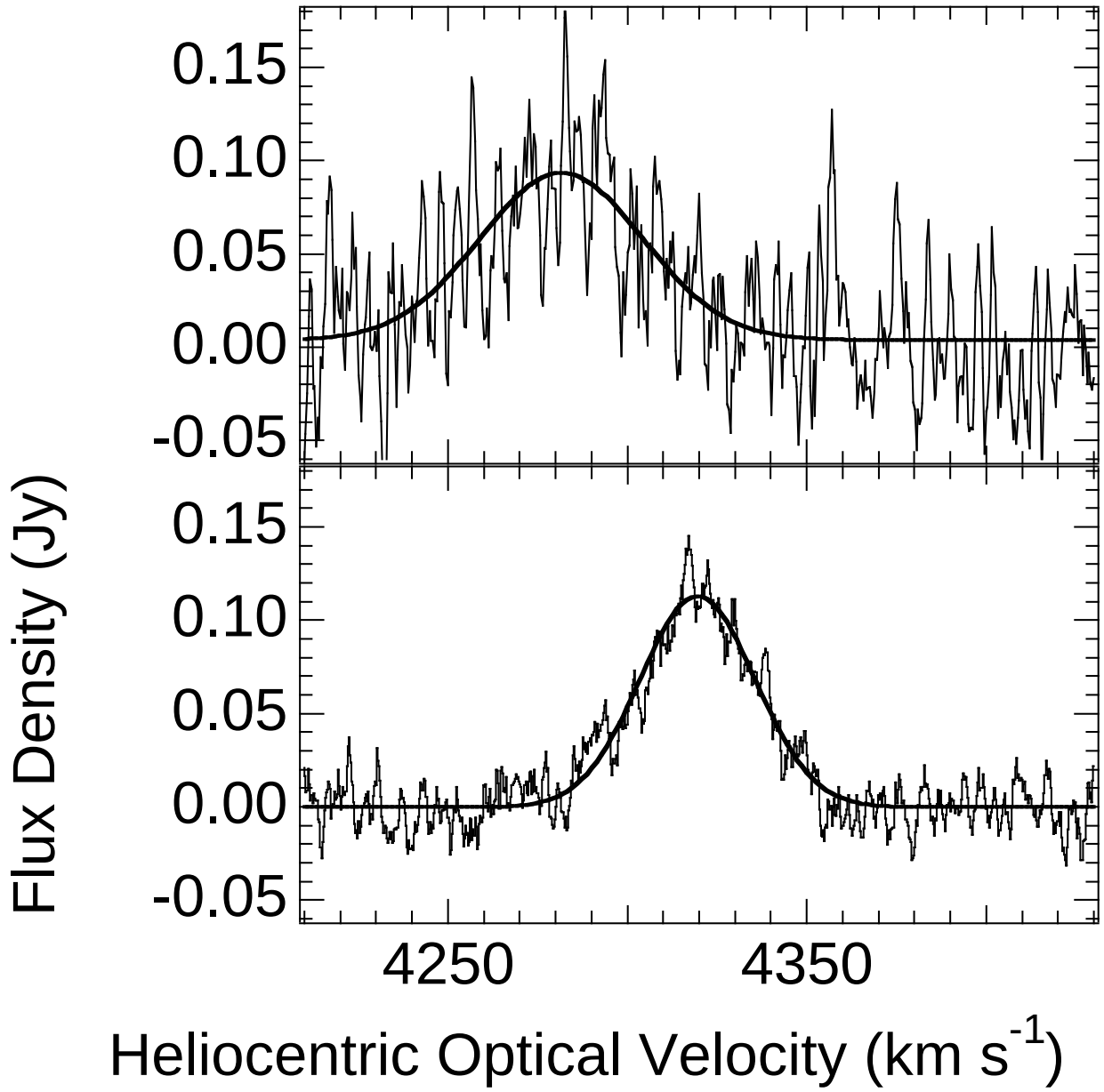

Fig. 2.— Spectra of H_2O maser emission in IRAS F01063-8034. *(top)*– Discovery spectrum obtained with the Parkes telescope, convolved with a 2.1 km s^{-1} wide boxcar function. *(bottom)*– Confirming spectrum obtained with the Tidbinbilla antenna 13 days later, convolved with a 1.9 km s^{-1} wide boxcar function. The curves are the fitted Gaussian line profiles whose parameters are listed in the text.

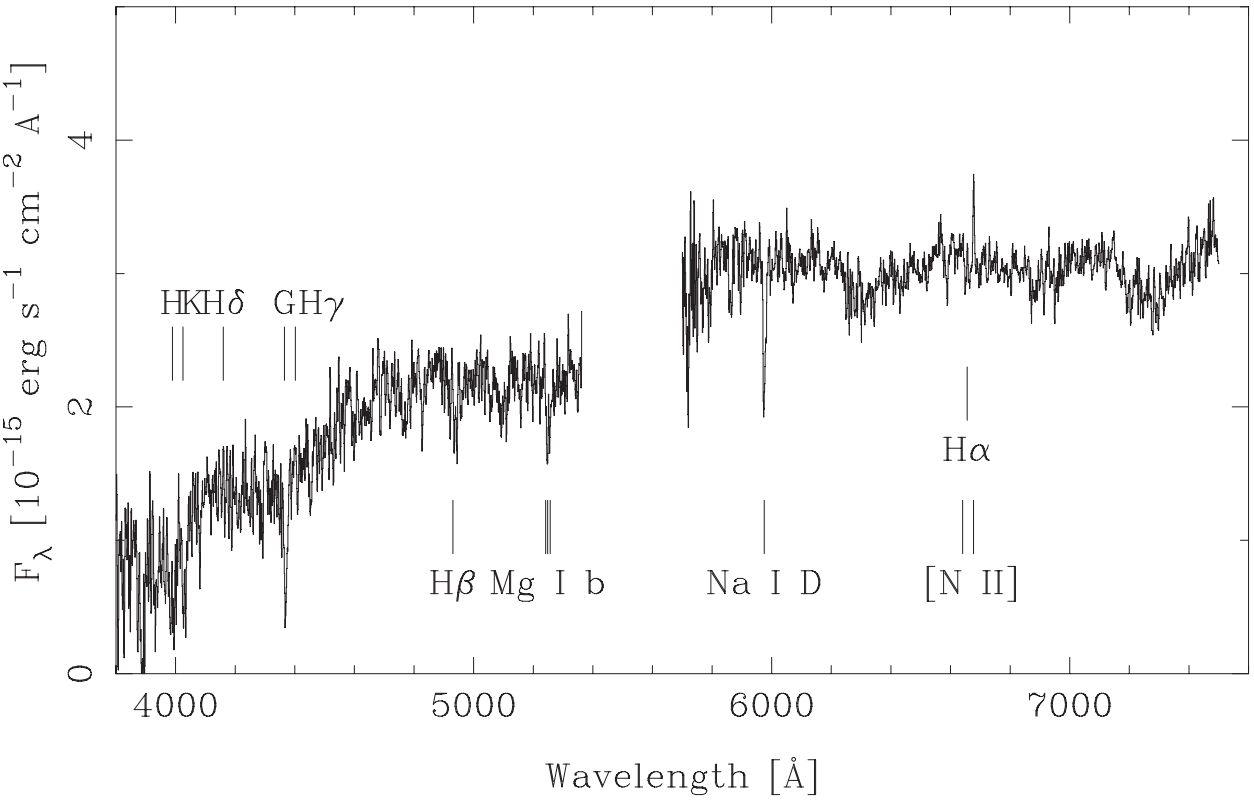

Fig. 3.— Blue and red optical spectra of IRAS F01063-8034. The vertical bars indicate the rest wavelengths of the Ca II H and K, G band, Mg I b, and Na I D absorption lines, as well as the Hα/[N II], and higher Balmer emission lines.

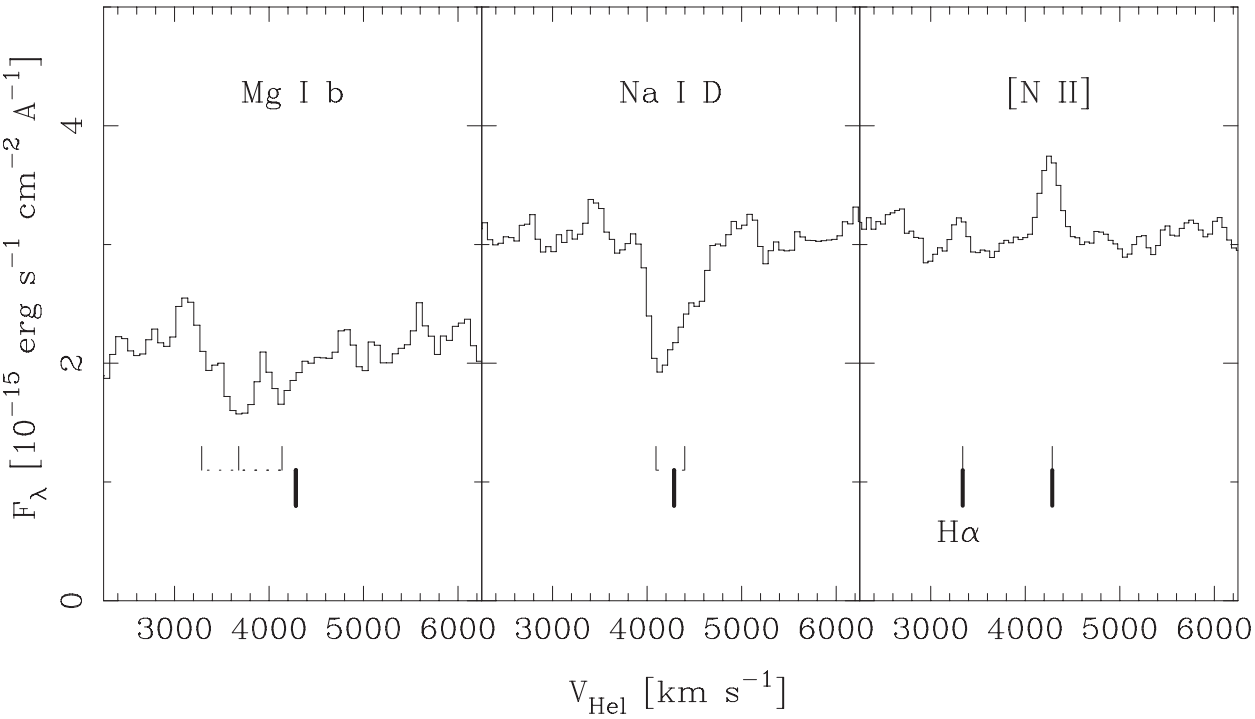

Fig. 4.— Line profiles of the Mg I b λ5183.3 and Na I D absorption lines, and the [N II] λ6583 emission line, plotted with respect to heliocentric velocity. Heavy vertical lines in each frame indicate a velocity of 4246 km s^{-1}. Light vertical lines denote spectral features of Mg I b $\lambda\lambda$5168,5175,5183, Na I D $\lambda\lambda$5889,5895, and Hα/[N II] λ6583.

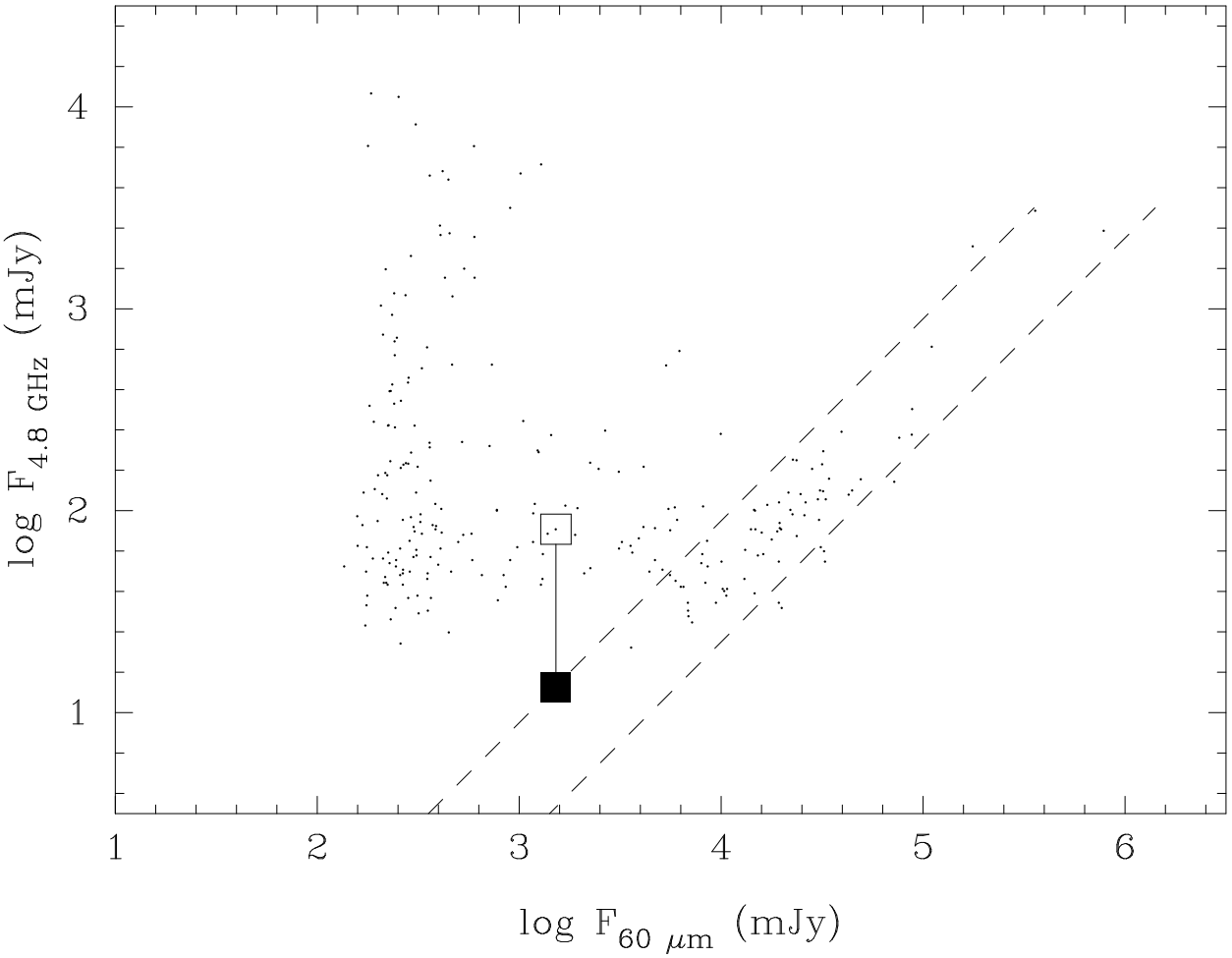

Fig. 5.— Radio-FIR diagram for sources found by correlating the 6.3 cm wavelength PMN catalog (Wright et al. 1994) with the IRAS 60μm Faint Source Catalog (Moshir et al. 1992). An *open square* indicates the position of IRAS F01063-8034 based on its PMN radio flux density. A *filled square* indicates the revised position based on the ATCA-measured radio flux density. *Dashed* lines represent the radio-FIR correlation for starbursts galaxies and radio-quiet AGNs.

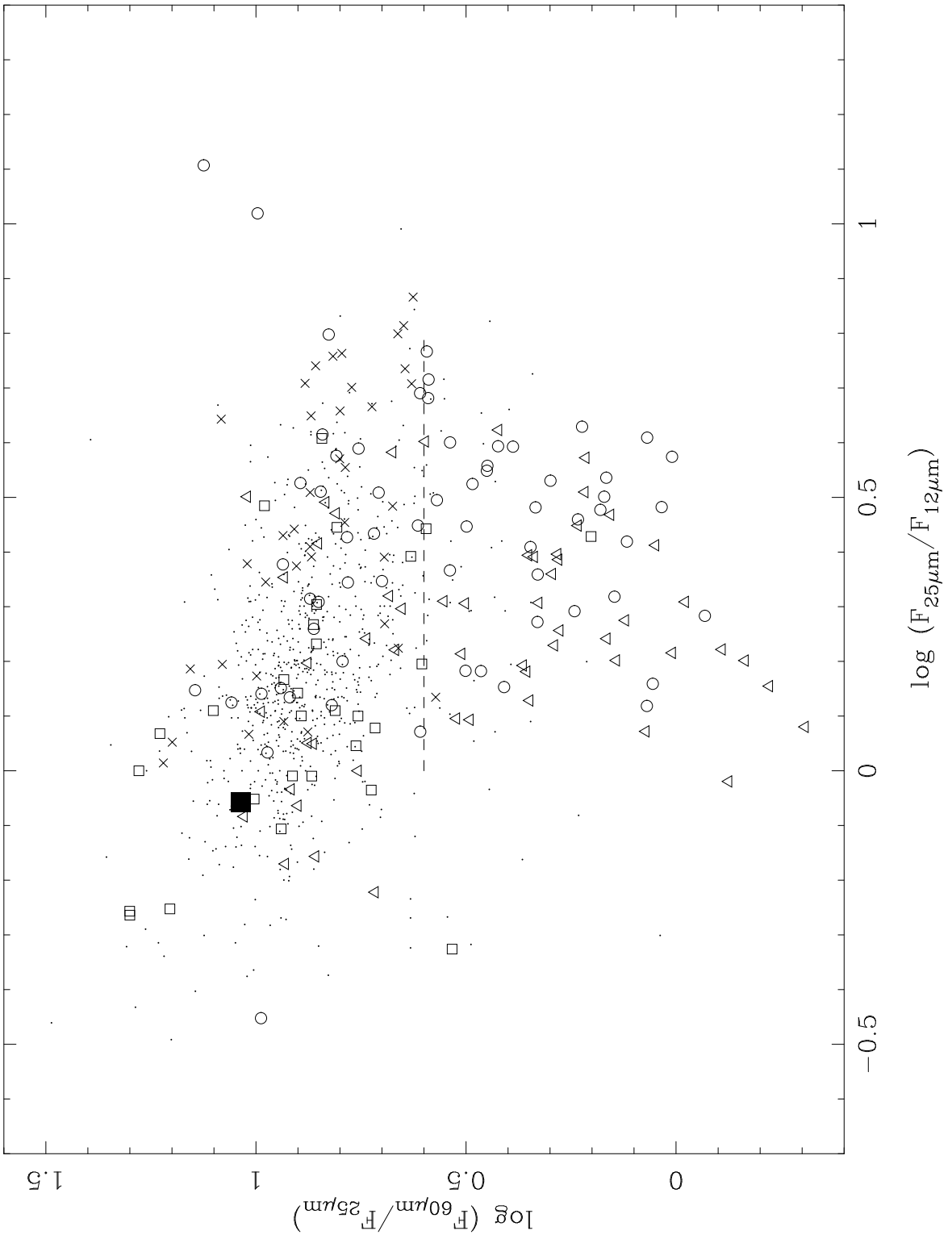

Fig. 6.— Far-infrared two color diagram based on data for the Extended 12 Micron Galaxy Sample of Rush et al. (1993). Seyfert 1 galaxies (*triangles*), Seyfert 2 galaxies (*circles*), LINER galaxies (*squares*), starburst galaxies (*crosses*), and normal galaxies (*points*) are indicated. The criterion of Low et al. (1988) for "warm extragalactic objects" ($\log(F_{60\mu m}/F_{25\mu m}) < 0.6$ is indicated by a *dashed line*. IRAS F01063-8034 is shown as a *filled square*.

Table 1. Observation Log

Dates	Receiver	T_{sys} (K)	Sensitivity[a] ($Jy\,K^{-1}$)	Calibration Unc.[b] (%)
1993 March 11-18	Maser	70-110	5.7	30
1995 October 11-16	HEMT	70-250[c]	5.7	30
1996 September 11-15	HEMT	100 [d]	8.5	50
1997 July 21-29	HEMT	100	8.4	30
1998 August 24-28	HEMT	110	6.3	20-30

[a]Sensitivity of the illuminated central 44m of the antenna. The sensitivities estimated in 1993 and 1997 were adopted to calibrate the data obtained in 1995 and 1996, respectively. The sensitivity changed significantly between 1995 and 1996 and between 1997 and 1998 because of antenna modifications.

[b]Overall uncertainty in flux density calibration.

[c]System temperature of prototype receiver increased with redshift. The maximum corresponds to sky frequencies ~ 21 GHz.

[d]T_{sys} uncertain by 50%.

Table 2. Observations at Parkes

Source	Alias	RA(1950)	Dec(1950)[a]	Morphology[b]	V_{sys}[c] (km s^{-1})		Velocity Range[d] (km s^{-1})		RMS Range[e] (Jy)		Epoch
NGC 55[f]	···	00 12 38.00	−39 29 54.0	SB(s)m: sp	129	±3	−302	561	0.11	0.13	1993
IRAS F00198-7926	···	00 19 55.6	−79 26 52	pec Sy2	21825	30	20013	22536	0.075	0.090	1997
IRAS F00198-7926	···	00 19 55.60	−79 26 52	pec Sy2	21825	30	21180	22472	0.057	0.10	1995
IRAS F00344-3349	ESO 350-IG038	00 34 25.67	−33 49 49.0	triple	6154	67	5570	6739	0.068	0.074	1995
IRAS F00494-3056	···	00 49 26.82	−30 56 18.2	SAB(r)ab	15529	120	14909	16151	0.13	0.17	1995
IRAS F00521-7054	···	00 52 06.38	−70 54 18.9	E/S0 Sy2	20656	30	20344	21629	0.063	0.10	1995
NGC 300[f]	···	00 52 31.75	−37 57 15.1	SA(s)d	144	1	−132	733	0.086	0.11	1993
NGC 334	···	00 56 27.83	−35 23 04.9	(R′)SB(s)b pec:	9210	10	7574	10275	0.096	0.13	1997
IRAS F01063-8034	ESO 013-G012	01 06 21.00	−80 34 24.0	Sa	5045[g]	26	4465	5626	0.057	0.063	1995
IRAS F01063-8034	ESO 013-G012	01 06 21.00	−80 34 24.0	Sa	4249[g]	21	3084	6181	0.25	0.26	1998
IC 1631	IRAS F01065-4644	01 06 31.60	−46 44 31.9	Sab pec Sy2	9246	49	8913	9594	0.049	···	1996
NGC 424[h]	···	01 09 09.64	−38 20 56.8	(R)SB(r)0/a Sy2	3496	30	1583	4825	0.09	0.15	1997
IC 1657[h]	···	01 11 46.57	−32 54 55.1	(R′)SB(s)bc Sy2	3552	10	1652	4881	0.066	0.084	1997
IRAS 01196-3254	···	01 19 35.40	−32 54 25.0	S0	9300	95	8699	9892	0.068	0.074	1995
NGC 526	···	01 21 38.00	−35 19 42.0	pair	5762	52	5180	6346	0.051	0.063	1995
NGC 625	···	01 32 54.10	−41 41 34.2	SB(s)m? sp	405	5	−28	837	0.048	···	1993
IRAS F01363-4016	ESO 297-G018	01 36 26.68	−40 15 53.8	Sa: sp Sy2	7555	15	7226	7899	0.039	···	1996
MCG-01-05-031	IRAS F01428-0404	01 42 53.50	−04 04 37.0	SB(rs)bc pec: Sy2	5456	22	3535	6632	0.12	0.14	1998
AM 0142-435	ESO 245-G005	01 42 58.00	−43 50 54.0	IB(s)m	395	6	−37	828	0.096	···	1993
Fairall 377	ESO 197-G027	02 09 01.25	−49 56 01.4	S Sy2	14240	90	13625	14857	0.13	0.17	1995
NGC 1032	···	02 36 49.09	+00 52 44.5	S0/a	2694	18	1112	4228	0.13	0.14	1998
IC 1858	···	02 47 01.96	−31 29 46.0	SA0+:	6070	15	4514	7611	0.12	0.14	1998
NGC 1125[h]	···	02 49 20.31	−16 51 19.7	(R′)SAB(rl:)0$^+$ Sy2	3297	22	1381	4625	0.093	0.16	1997
MCG -02-08-039	···	02 58 05.70	−11 36 50.0	SAB(rs)a pec: Sy2	8874	90	7270	9969	0.066	0.075	1997
NGC 1194	···	03 01 16.45	−01 17 53.8	SA0+: Sy1	4015	30	3695	4353	0.045	···	1996
NGC 1209	···	03 03 42.80	−15 48 14.0	E6:	2600	18	2254	2988	0.045	···	1996
IRAS F03106-0254	···	03 10 37.49	−02 54 28.0	S0 Sy2	8154	90	7563	8747	0.086	0.091	1995
IRAS 03125+0119	···	03 12 30.35	+01 19 25.5	Sy2	7200	70	6612	7789	0.095	0.11[i]	1995
NGC 1313	···	03 17 39.00	−66 40 42.0	SB(s)d HII	475	3	25	890	0.062	···	1993
IRAS F03278-4329	···	03 27 48.69	−43 29 24.6	Sy2	17508	90	16880	18138	0.13	0.17	1995
NGC 1365[g]	···	03 31 41.80	−36 18 26.6	(R′)SBb(s)b Sy1.8	1636	1	−228	2982	0.084	0.08	1997
NGC 1448	···	03 42 52.70	−44 48 05.0	SAcd: sp	1164	5	730	1599	0.10	···	1993

Table 2—Continued

Source	Alias	RA(1950)	Dec(1950)[a]	Morphology[b]	V_{sys}[c] ($km\,s^{-1}$)		Velocity Range[d] ($km\,s^{-1}$)		RMS Range[e] (Jy)		Epoch
ESO 549-G040	···	03 54 56.09	−18 55 16.3	Sb-c	7534	10	5970	8655	0.096	0.12	1997
3C98	···	03 56 10.20	+10 17 32.0	E1?	9130	42	7376	10075	0.060	0.072	1997
IRAS F04023-1638	···	04 02 21.5	−16 38 27	···	8694	150	8686	10286	0.17	0.18[i]	1998
NGC 1587	II Zw 012	04 28 05.50	+00 33 16.9	E pec	3694	12	3332	4071	0.035	···	1996
ESO 552-G004	···	04 45 17.08	−17 41 05.1	SA(rl)0^0	9007	20	7376	10075	0.058	0.099	1997
ESO 485-G016	···	04 46 50.31	−23 49 00.8	SAB(rs)ab:	8129	22	6503	9174	0.07	0.12	1997
NGC 1684	···	04 50 00.80	−03 11 20.0	E+ pec:	4456	25	2933	6085	0.13	0.14	1998
NGC 1705	···	04 53 06.20	−53 26 27.0	SA0- pec: HII	628	9	240	1107	0.10	···	1993
NGC 1808	···	05 05 58.58	−37 34 36.5	(R′)SAB(s:)b Sy2	1000	5	566	1435	0.087	···	1993
NGC 1808[g]	···	05 05 58.58	−37 34 36.5	(R′)SAB(s:)b Sy2	1000	5	−1001	2445	0.078	0.11	1997
IRAS F05189-2524	···	05 18 58.90	−25 24 39.0	pec Sy2	12760	54	12150	13370	0.11	0.11	1995
ESO 253-G003	···	05 23 53.00	−46 02 54.0	Sa? Sy2	12747	21	10589	13280	0.09	0.10	1997
IRAS F05238-4602	ESO 253-G003	05 23 53.00	−46 02 54.0	Sa? Sy2	12738	22	12099	13319	0.11	0.11	1995
IC 422	···	05 30 05.15	−17 15 34.5	···	2698	150	1218	4294	0.13	0.11	1998
EXO 0556.3-3820	IRAS F05563-3820	05 56 21.10	−38 20 17.1	Sy1	10154	180	9728	10929	0.068	0.08	1995
NGC 2207	···	06 14 14.40	−21 21 14.0	SAB(rs)bc pec	2741	15	2361	3240	0.11[i]	···	1993
ESO 491-G021	···	07 07 49.00	−27 29 36.0	SB(r)ab? pec	2847	68	2361	3240	0.11[i]	···	1993
NGC 2369	···	07 16 05.00	−62 15 12.0	(R′_2)SAB(s)ab	3237	36	2660	3541	0.10[i]	···	1993
NGC 2442	···	07 36 33.13	−69 24 58.3	SAB(s)bc pec	1449	7	863	1997	0.089	0.089	1995
ESO 495-G021	He 2-010	08 34 07.00	−26 14 06.0	I0? pec starburst	873	1	440	1308	0.084	···	1993
NGC 2623	Arp 243	08 35 25.18	+25 55 50.7	LINER, triple	5535	8	4954	6118	0.051	0.057	1995
NGC 2640	···	08 36 05.00	−54 56 51.0	SA0⁻	1051	32	736	1381	0.11	···	1996
NGC 2835	···	09 15 37.00	−22 08 42.0	SAB(rs)c	888	5	455	1323	0.086	···	1993
NGC 2845	···	09 16 37.00	−37 48 00.0	SA(rs)a Sy2	2530	6	2212	2863	0.041[i]	···	1996
IRAS F09182-0750	MCG -01-24-012	09 18 18.58	−07 50 35.4	SAB(rs)c: Sy2	5936	90	5353	6520	0.12	0.12	1995
NGC 2915	···	09 26 31.00	−76 24 30.0	I0	468	5	36	901	0.098	···	1993
NGC 2997[f]	···	09 43 27.35	−30 57 32.8	SA(s)c	1087	4	653	1522	0.13	···	1993
ESO 434-G040	···	09 45 28.43	−30 42 57.0	(RL)SA(l)0$\hat{0}$ Sy2	2482	42	590	3806	0.093	0.10	1997
ESO 373-G29[h]	···	09 45 33.10	−32 36 18.0	(R)SAB(r)a Sy2	2802	10	886	4125	0.058	0.090	1997
NGC 3059	···	09 49 38.00	−73 41 12.0	SB(rs)c	1260	6	826	1696	0.089[i]	···	1993
NGC 3078	···	09 56 08.10	−26 41 13.0	E2-3	2495	25	2136	2869	0.032	···	1996
NGC 3109[f]	···	10 00 49.00	−25 55 00.0	SB(s)m	403	1	68	934	0.1	0.14	1993
IC 2545	···	10 03 53.00	−33 38 30.0	···	10267	86	8573	11334	0.07	0.075	1997

Table 2—Continued

Source	Alias	RA(1950)	Dec(1950)[a]	Morphology[b]	V_{sys}[c] ($km\,s^{-1}$)		Velocity Range[d] ($km\,s^{-1}$)		RMS Range[e] (Jy)		Epoch
IC 2554	···	10 07 30.20	−66 47 02.0	SB(s)bc pec: pair?	1474	30	943	1814	0.12[i]	···	1993
FAIRALL 1149[h]	···	10 11 08.00	−35 44 06.0	(R′_2)SB(s)ab Sy2	8530	14	6897	9592	0.058	0.093	1997
NGC 3175	···	10 12 25.00	−28 37 24.0	SAB(s)b	1101	5	661	1530	0.048[i]	···	1993
ESO 317-G023	···	10 22 31.00	−39 03 06.0	(R′_1)SB(rs)a	2892	19	2453	3332	0.085[i]	···	1993
NGC 3256	···	10 25 43.40	−43 38 48.0	Pec merger starburst	2738	28	2299	3178	0.080[i]	···	1993
NGC 3281	···	10 29 35.90	−34 35 46.0	SAB(rs+)a Sy2	3200	22	3059	3942	0.083[i]	···	1993
NGC 3281[h]	···	10 29 35.90	−34 35 46.0	SAB(rs+)a Sy2	3200	22	1543	4789	0.078	0.099	1997
IRAS F10329-1352	MCG-02-27-009	10 32 59.60	−13 52 14.0	SB(rs)0+ pec? Sy2	4529	31	4165	4908	0.023	···	1996
MCG-02-27-009	IRAS F10329-1351	10 32 59.60	−13 52 14.0	SB(rs)0+ pec? Sy2	4529	31	3092	6189	0.12	0.15	1998
NGC 3511	···	11 00 57.00	−22 49 00.0	SAB(s)c Sy1	1106	4	672	1541	0.088	···	1993
ESO 438-G020	···	11 16 27.00	−29 09 06.0	S? LINER	9121	10	7435	10075	0.087	0.12	1997
IRAS F11186-0242	···	11 18 39.08	−02 42 36.5	SAB(s)b HII Sy2	7464	23	6875	8054	0.051	0.057[i]	1995
ESO 320-G030	Fairall 1151	11 50 39.90	−38 51 07.0	(R′_1)SAB(r)a NELG	3232	19	2660	3541	0.094	···	1993
NGC 4507[h]	···	12 32 54.50	−39 38 02.0	SAB(s)ab Sy2	3538	9	1606	4832	0.096	0.14	1997
M 104	Sombrero	12 37 23.39	−11 20 54.9	SA(s)a LINER Sy1.9	1024	5	−504	2596	0.13	0.15	1998
IC 3639[h]	···	12 38 10.60	−36 28 54.0	SB(rs)bc: Sy2	3275	7	1394	4527	0.06	0.12	1997
ESO 172-G010[h]	···	12 44 46.3	−53 16 41	SBm	1829	30	−80	3171	0.070	0.072	1997
IRAS F12585-3208	ESO 443-G029	12 58 36.00	−32 07 54.0	SA(r)c	9397	24	7912	9411	0.11	0.11	1997
ESO 508-G05[h]	···	13 04 14.00	−23 39 00.0	SB(rl)0/a:	2947	40	1052	4253	0.081	0.11	1997
NGC 4968[h]	···	13 04 24.00	−23 24 42.0	(R′)SAB0$\hat{0}$ Sy2	2957	26	1052	4243	0.13	0.14	1997
IRAS F13109-1509	···	13 10 54.8	−15 10 00	SAB(s)dm	2502	6	910	4036	0.12	0.14	1998
NGC 5068	···	13 16 12.10	−20 46 36.0	SB(s)d	673	5	566	1435	0.082	···	1993
NGC 5078	···	13 17 04.84	−27 08 50.4	SA(s)a: sp	2168	6	567	3660	0.19	0.29	1998
IRAS F13174-1651	VV802	13 17 25.9	−16 51 13	pair	6296	150	4704	7801	0.15	0.15	1998
ESO 324-G024	UKS 1324-412	13 24 42.00	−41 13 18.0	IABm:	513	6	81	947	0.12[i]	···	1993
M 83[f]	···	13 34 11.55	−29 36 42.2	SAB(s)c HII starburst	516	4	45	910	0.097	0.099	1993
NGC 5253	···	13 37 05.12	−31 23 13.2	Im pec HII starburst	404	4	−28	837	0.14	···	1993
ESO 221-IG010	···	13 47 48.00	−48 48 30.0	pair	3099	39	2588	3469	0.096[i]	···	1993
NGC 5495	IRAS F14095-2652	14 09 31.00	−26 52 24.0	(R′)SA(rs)b Sy2	6737	9	6370	7125	0.032	···	1996
UKS 1424-460	···	14 24 48.00	−46 04 48.0	IB(s)m	397	68	−39	826	0.093	···	1993
NGC 5643	···	14 29 27.30	−43 57 16.0	SAB(rs)c Sy2	1199	5	666	1535	0.059	···	1993
NGC 5643[h]	···	14 29 27.30	−43 57 16.0	SAB(rs)c Sy2	1199	5	−706	2528	0.070	0.087	1997
NGC 5833	···	15 06 42.00	−72 40 12.0	SAB(r)c	3071	8	2590	3471	0.10[i]	···	1993

Table 2—Continued

Source	Alias	RA(1950)	Dec(1950)[a]	Morphology[b]	V_{sys}[c] ($km\,s^{-1}$)		Velocity Range[d] ($km\,s^{-1}$)		RMS Range[e] (Jy)		Epoch
IRAS F15366+0544	ARK481	15 36 36.77	+05 43 58.9	E	7781	42	6181	9283	0.15	0.17	1998
IRAS 15374-1817	ESO 583-G002	15 37 28.6	−18 16 55	SB(rs)bc Sy1	7042	10	6724	7395	0.037	···	1996
IRAS 15480-0344	···	15 48 03.98	−03 44 17.5	S0 Sy2	9084	90	8489	9680	0.068	0.074[i]	1995
3C327	IRAS F15599+0206	15 59 55.67	+02 06 12.3	Sy2	31170	150	30495	31863	0.044	0.063	1995
NGC 6156	···	16 30 28.60	−60 30 53.0	(R′)SAB(rs)c	3300	30	2660	3541	0.069[i]	···	1993
ESO 137-G034	···	16 31 01.00	−57 58 30.0	SAB(s)0/a? Sy2	2747	16	2411	3290	0.093[i]	···	1993
NGC 6215	···	16 46 47.43	−58 54 26.5	SA(s)c pec	1560	6	915	1786	0.079	···	1993
NGC 6221	···	16 48 25.40	−59 08 00.0	SB(s)bc pec Sy2	1482	6	915	1786	0.079	···	1993
NGC 6300	···	17 12 18.00	−62 45 54.0	SB(rs)b Sy2	1110	6	676	1545	0.059	···	1993
IC 4662	He 2-269	17 42 12.00	−64 37 18.0	IBm	308	4	−125	740	0.077	···	1993
IRAS F18325-5926	Fairall 49	18 32 32.49	−59 26 40.2	Sa Sy2	6065	70	5481	6650	0.046	0.051	1995
H1846-786	IRAS F18389-7834	18 39 03.5	−78 35 06	Sy1	22275	15	22135	23435	0.046	0.074	1995
IC 4778	···	18 45 25.00	−61 46 36.0	(R′)SB(s)a	4971	45	3388	6481	0.13	0.15	1998
NGC 6753	···	19 07 11.00	−57 07 54.0	(R)SA(r)b	3124	26	2660	3541	0.098	···	1993
IRAS F19254-7245	Super Antenna	19 25 29.86	−72 45 37.5	pair	18500	80	17868	19133	0.091	0.11	1995
IRAS F19254-7245	Super Antenna	19 25 29.86	−72 45 37.5	pair	18500	80	16926	20018	0.15	0.15	1998
IRAS F19254-7245	Super Antenna	19 25 29.86	−72 45 37.5	pair	18500	80	17704	19299	0.072	0.075	1997
IC 4859	···	19 25 52.00	−66 25 18.0	SA(s)bc	5003		4424	5584	0.063	0.076	1995
NGC 6810	IRAS F19393-5846	19 39 21.00	−58 46 30	SA(s)ab:sp Sy2	2031	10	1714	2363	0.043	···	1996
NGC 6810	···	19 39 21.00	−58 46 30.0	SA(s)ab:sp Sy2	2031	10	383	3471	0.12	0.12	1998
IRAS F19395-7000	ESO 073-G005	19 39 35.00	−70 00 12.0	SAa?	3786		2215	5304	0.13	0.13	1998
NGC 6868	···	20 06 16.40	−48 31 39.0	E2	2854	15	2638	3346	0.076	0.076	1995
IC 5052	···	20 47 22.00	−69 23 30.0	SBd: sp	598	5	165	1032	0.11	···	1993
ESO 286-G018[j]	IRAS F20545-4334	20 54 30.30	−43 34 10.2	SB(s)bc? Sp	9147	10	8552	9744[k]	0.11	0.13[i]	1995
NGC 6987	···	20 54 41.55	−48 49 25.0	E0:	5239	27	4889	5636	0.023	···	1996
IRAS F20559-5251	ESO 187-G042	20 55 54.65	−52 51 33.1	(R′)SB(s)a Sy2	7180	36	6852	7523	0.038	···	1996
Mrk 897	···	21 05 15.07	+03 40 31.9	Sy2	7897	1	7176	8667	0.066	0.070	1997
IRAS F21497-0824	···	21 49 47.20	−08 24 31.8	···	10330	41	7952	11871	0.15	0.17	1998
IRAS F21529-6955	ESO 075-G041	21 52 58.00	−69 55 41.2	SA0- Radio gal Sy2	8476	31	6907	9168	0.15	0.17	1998
IC 5152[f]	···	21 59 26.58	−51 32 14.5	IA(s)m	124	3	−157	708	0.099	0.046	1993
NGC 7205	···	22 05 10.80	−57 41 16.0	SA(s)bc LINER	1690	7	915	1786	0.08	···	1993
NGC 7213	···	22 06 08.40	−47 24 45.0	SA(s)0$\hat{0}$ Sy1.5	1792	9	1225	2361	0.095	0.10	1995
3C445	···	22 21 14.72	−02 21 25.3	N BLRG Sy1	16848	15	16223	17475	0.12	0.14	1995

Table 2—Continued

Source	Alias	RA(1950)	Dec(1950)[a]	Morphology[b]	V_{sys}[c] ($km\,s^{-1}$)		Velocity Range[d] ($km\,s^{-1}$)		RMS Range[e] (Jy)		Epoch
NGC 7410[h]	···	22 52 09.74	−39 55 45.0	SB(s)a LINER Sy2	1751	28	−158	3071	0.099	0.12	1997
NGC 7410	···	22 52 11.00	−39 55 42.0	SB(s)a LINER Sy2	1751	28	166	1798	0.13	0.14	1998
IC 1459	IRAS F22544-3643	22 54 23.11	−36 43 47.4	E3	1691	18	138	3236	0.13	0.14	1998
IC 1459	···	22 54 23.11	−36 43 47.4	E3	1691	18	1374	2022	0.068[i]	···	1996
IRAS F23031-3052	ESO 469-G011	23 03 05.60	−30 52 55.0	pec Sy2	8504	13	8274	8951	0.043	···	1996
ESO 407-G018	UKS 2323-326	23 23 47.29	−32 39 50.4	IB(s)m pec:	62	5	−369	494	0.055	···	1993
IRAS F23377-4447	ESO 292-G009	23 37 44.45	−44 47 30.9	SAB(r)b Sy	15444	20	14825	16066	0.13	0.18	1995
ESO 471-G006	AM 2341-321	23 41 08.53	−32 14 01.5	SB(s)m: sp	267	8	−105	760	0.076	···	1993
NGC 7793[f]	···	23 55 15.50	−32 52 03.0	SA(s)d	230	2	−132	733	0.077	0.084	1993
IRAS F23565-7631	···	23 56 30.5	−76 31 19	···	25183	150	23625	26715	0.21	0.29	1998

[a] Catalog coordinates listed by NED. Pointing positions differed by > 10% of the 1′.4 beam (half-power full-width) in 10 cases– IRAS F09182-0750 (13″.1), IRAS F13109-1509 (13″.1), IRAS F23377-4447 (8″.4), NGC 625 (24″.0), NGC 3621 (11″.1), NGC 5128 (12″.6), NGC 5253 (17″.8), NGC 5643 (8″.5), NGC 7410 (9″.5), and NGC 7793 (9″.5).

[b] Optical morphology as listed by NED, largely following the notation of de Vaucouleurs, de Vaucouleurs, & Corwin (1976).

[c] Heliocentric velocity referenced by NED, assuming the optical definition of Doppler shift.

[d] Velocities corresponding to the highest and lowest observed frequencies. Excludes guard bands of 2 MHz in 1997 and 1998, and 5 MHz in 1996, in which the effects of filter roll-off can be severe.

[e] RMS noise level in a 0.84 km s^{-1} spectral channel after Hanning smoothing.

[f] Multiple fields observed: 10 in NGC 55, 5 in NGC 300, 2 in NGC 2997, 8 in NGC 3109, 36 in M 83, 14 in NGC 7793, and 6 in IC 5152.

[g] Estimates of systemic velocity in the literature disagree. See review in §3.2.

[h] Object previously observed with a roughly 600 km s^{-1} bandwidth centered on the systemic velocity. No emission reported. Observations reported here cover velocities red and blueshifted outside that band. Quoted velocity range reflects composite of old and new observations.

[i] Reduced pointing accuracy due to high winds or attentuation due to overcast may have degraded sensitivity.

[j] Paired with ESO 286-G017 at 9778 ± 5 km s^{-1}, which is type Sy2.

[k] Velocities between 9408 and 9475 km s^{-1} not observed.

Table 3. Properties of IRAS F01063-8034

Measurement		Ref.
Alias	ESO 013-G012	
Hubble Type	Sa	
Optical α_{2000}	$01^h07^m01^s \pm 3''$	1
δ_{2000}	$-80°18'24'' \pm 8''$	
λ6cm α_{2000}	$01^h07^m01\overset{s}{.}70 \pm 0\overset{s}{.}4$	2
δ_{2000}	$-80°18'28\overset{''}{.}1 \pm 1''$	
Position Angle	$153° \pm 2°$ [(a)]	
Inclination	$83°$ [(b)]	
$V_{\rm sys}$	5047 ± 21 km s^{-1} [(c)]	3
	4249 ± 27 km s^{-1}	4
	4285 ± 35 km s^{-1}	5
F_ν (12 μm)	0.16 ± 0.02 Jy	6
F_ν (25 μm)	0.14 ± 0.02 Jy	6
F_ν (60 μm)	1.52 ± 0.06 Jy	6
F_ν (100 μm)	6.51 ± 0.3 Jy	6
F_ν (λ6.3 cm)	13.4 ± 0.4 mJy [(d)]	2
F_ν (λ3.5 cm)	11.7 ± 0.4 mJy [(d)]	2
F_ν (λ13 cm)	< 4 mJy [(e)]	7

[(a)] Position angle estimated from Figure 1.

[(b)] Inclination estimated from the axial ratio of isophotes (van den Bergh 1988).

[(c)] Systemic heliocentric velocities, assuming the optical definition of Doppler shift.

[(d)] Integrated flux density. Beam half-power full width 1 - 2″.

[(e)] Fringe spacing of interferometric observation 0″.09.

References. — 1: ESO/Uppsala Survey, 2: McGregor et al., in prep., 3: Sadler (1984), 4: Dacosta et al. (1991), 5: this work, 6: Moshir et al. (1992), 7: Slee et al. (1994).